UNIVERSIDAD NACIONAL DE COLOMBIA
SEDE MEDELLÍN
FACULTAD DE MINAS

DYNA
http://dyna.medellin.unal.edu.co/

Glow discharge effect on temperature and time of treatment for the synthesis of Mo-doped manganite

Iván Supelano-García [a], Willian Arnulfo Aperador-Chaparro [b], Carlos Arturo Parra-Vargas [a] & Armando Sarmiento-Santos [a]

[a] *Facultad de Ciencias, Universidad Pedagógica y Tecnológica de Colombia, Tunja, Colombia. ivan.supelano@uptc.edu.co, carlos.parra@uptc.edu.co, asarmiento.santos@uptc.edu.co*
[b] *Facultad de Ingeniería, Universidad Militar Nueva Granada, Bogotá, Colombia. william.aperador@unimilitar.edu.co*

Received: February 13th, 2019. Received in revised form: March 27st, 2019. Accepted: April 15th, 2019.

Abstract
We report the synthesis of $CaMn_{0.9}Mo_{0.1}O_3$ manganite by glow discharge (GD) plasma treatment under Argon-Air atmosphere. The morphological, structural and magnetic properties were evaluated by scanning electron microscopy (SEM), X-ray diffraction (XRD) and magnetization measures. The results from these measures reveal that the properties of GD synthesized manganite are similar to that exhibited by $CaMn_{0.9}Mo_{0.1}O_3$ produced by conventional resistive furnace. The Rietveld analysis of XRD patterns performed at room temperature show that the samples crystallize in orthorhombic structure of Pnma (62) space group. The magnetization curves as a function of temperature show two inflection points related to paramagnetic-antiferromagnetic and structural transition. The GD treatment produces a compound with similar properties, reducing the time and energy consumption in comparison with conventional synthesis route by using resistive furnace.

Keywords: glow discharge; manganite; magnetic properties; structural properties.

Efecto de la descarga luminiscente en la temperatura y el tiempo de tratamiento para la síntesis de manganita dopada con Mo

Resumen
En este trabajo reportamos la síntesis de la manganita $CaMn_{0.9}Mo_{0.1}O_3$ empleando plasma de descarga luminiscente en atmosfera de argón-aire. Se evaluaron las propiedades morfológicas, estructurales y magnéticas a través de microscopía electrónica de barrido (MEB), difracción de rayos X (DRX) y medidas de magnetización. Los resultados de éstas medidas revelan que las propiedades de la manganita $CaMn_{0.9}Mo_{0.1}O_3$ sintetizada por descarga luminiscente son similares a las propiedades de la misma producida en horno resistivo convencional. El análisis Rietveld de los patrones de DRX tomados a temperatura ambiente revelan que la muestra cristaliza en el grupo espacial Pnma (62) ortorrómbica. Las curvas de magnetización en función de la temperatura muestran dos puntos de inflexión que evidencian una transición paramagnética-antiferromagnética y una transición estructural. El tratamiento por descarga luminiscente produce un compuesto con propiedades similares, reduciendo el tiempo y consumo energético en comparación con la producción del mismo material usando horno resistivo.

Palabras clave: descarga luminiscente; manganita; propiedades magnéticas; propiedades estructurales.

1. Introduction

Manganites with perovskite-like structure $AMnO_3$ have been studied extensively due to their remarkable and wide range of physical properties, such as magnetocaloric effect [1,2], colossal magnetoresistance [3,4] and insulator-metal transition [5,6]. Amid manganites, the $CaMn_{0.9}Mo_{0.1}O_3$ (CMMO) based on $CaMnO_3$ has been synthesized as single crystal [7] and polycrystalline [8]. $CaMnO_3$ crystallizes in orthorhombic structure at room temperature, it exhibits antiferromagnetic

How to cite: Supelano-García, I. , Aperador-Chaparro, W.A., Parra-Vargas, C.A. and Sarmiento-Santos, A., Glow discharge effect on temperature and time of treatment for the synthesis of Mo-doped manganite. DYNA, 86(209), pp. 225-229, April - June, 2019.

(AFM) G-type ordering and Neel temperature (T_N) at 130 K [9]. The CMMO displays an orthorhombic to monoclinic structural transition (Pnma - P21/m) at T_E=283 K, due to an ordering of the occupied e_g orbitals inside equatorial planes. The CMMO exhibits AFM-C type ordering at T_N=165 K [10]. The properties of perovskites can be affected by the synthesis route. For example, it is known that sintering of $La_{1-x}Mn_{1-x}O_3$ perovskite under oxygen atmosphere varies the Mn^{3+}/Mn^{4+} ratio, changing the electrical and magnetic properties [11].The most popular synthesis route to produce CMMO is the usual solid state reaction method in which the long time and high sintering temperatures of production are required to favor the grain growth. There are other routes to produce ceramic perovskites; for example, spark plasma sintering and thermal plasma assisted heating have been used to produce dense systems based on $LaMnO_3$ compound [12,13], the glow discharge (GD) has been applied in the sintering of materials [14]. According to the literature, the GD has been applied in diverse fields of science and technology, mainly in surface treatments, deposition processes, analytical techniques, heat transferring and sintering of materials [14,15].

In a previous paper [16], we have used the GD and a resistive furnace in the synthesis of CMMO. The aim of this work consists in the synthesis of CMMO by the sole use of GD and the evaluation of its structural, morphological and magnetic properties.

2. Materials and methods

The $CaMn_{0.9}Mo_{0.1}O_3$ perovskite was prepared with $CaCO_3$ (99.9999%), MnO_2 (99.99%), and MoO_2 (99%) oxides in powder. These oxides were dried, weighed in stoichiometric amounts, mixed and ground for 2 h in agate mortar. The mixture was compacted into a double effect cylindrical matrix. Finally, after several tests, the following synthesis conditions were set: a sample was heated at 700 ° C for 30 min, then, the sample was cooled and re-milled for one hour, finally it was compacted; subsequently, the sample was heated at 900 °C for 60 min; the sample obtained was labeled as CMMO-A. A second sample was synthesized by eliminating the intermediate grinding between heated treatments at 700 °C and 900 °C, the sample obtained was labeled as CMMO-B. The heating treatments were performed in GD using a reactor, the experimental setup is depicted in Fig. 1.

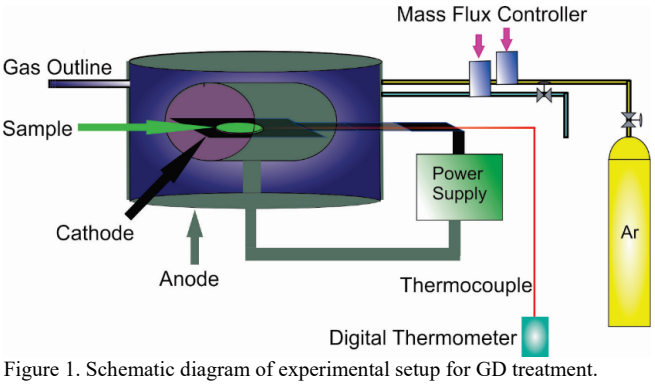

Figure 1. Schematic diagram of experimental setup for GD treatment. Source: The Authors.

The heating at 700 ° C was carried out under air in a controlled flow rate at 100 mL/min, with 460 V discharge voltage, 0.17 A discharge current and 2 Torr pressure; the heating at 900 °C was carried out under air (30%) -argon (70%) mixed flux with 550 V discharge voltage, 0.31 A discharge current and 3 Torr pressure. The heating/cooling rate was adjusted to 22.5 °C/min.

The crystal structure was studied with Rietveld refinement of X-ray diffraction (XRD) pattern using the GSAS software, the measurement was performed at room temperature using a PANalytical X'Pert's X-ray diffractometer with $K_{\alpha\text{-}Cu}$ radiation (λ = 1.54064 Å). The surface morphology was observed by scanning electron microscopy (SEM) with secondary electrons using a Zeiss electron microscope and composition was checked with EDS. Magnetic measurements of magnetization as a function of temperature were performed in the zero-field-cooled (ZFC) - field-cooled (FC) mode under magnetic applied field of 1 kOe; measurements of magnetization as a function of applied field were taken at 50 K with a VersaLab magnetometer of Quantum Design.

3. Results and discussion

In the previous study [16] the GD was used as supplement in the production of CMMO using a resistive furnace. In this study the parameters of GD were optimized to perform the synthesis without using a conventional resistive furnace. The XRD patterns taken at room temperature for CMMO-A and CMMO-B are displayed in Fig. 2. The samples show peaks corresponding to single phase. The data was analyzed by Rietveld analysis using the GSAS software, the refined patterns are shown in Fig. 3. The structural refinement was performed in an orthorhombic system with space group Pnma. Fitted parameters like atomic positions, lattice parameters and others are summarized in Table 1. The Jahn-Teller distortion of the MnO_6 octahedral was calculated using the equation [17]:

$$\sigma_{JT} = 10^3 \sqrt{((d_{Mn-O})_i - \langle d_{Mn-O}\rangle)^2 / 3} \quad (1)$$

where $(d_{Mn\text{-}O})_i$ is the Mn-O bond distance and $< d_{Mn\text{-}O} >$ is the average. The rotation angle θ_R and tilt angle θ_T were calculated as (90-ϕ)/2 and (180-θ)/2 respectively, in which ϕ is the angle among oxygen atoms on the ac plane and θ is the angle among Mn/Mo-Oap-Mn/Mo along b axis as is displayed in Fig. 4.

The results evidence a decreasing of a, b, and an increasing of c parameter for CMMO-A and CMMO-B in comparison with samples previously produced by conventional solid state reaction method using resistive furnace [8]. It is found that lattice parameters, cell volume, atomic positions, bond distances, bond angles and rotation angle for both samples CMMO-A and CMMO-B are very similar. The lattice parameters satisfy the $a \approx b/\sqrt{2} \approx c$ relation, it indicates a pseudocubic phase O* type. According to the Jahn-Teller distortion term and the absolute rotation angle, the values in CMMO-B are larger than in CMMO-A. From the above results it is concluding that both processes allow to

obtain the same crystal structure at room temperature with similar unit cell size and just a little variation in the rotation octahedral.

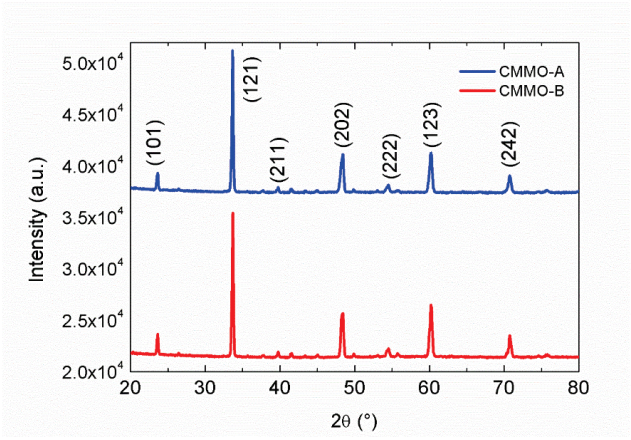

Figure 2. XRD patterns taken at room temperature.
Source: The Authors.

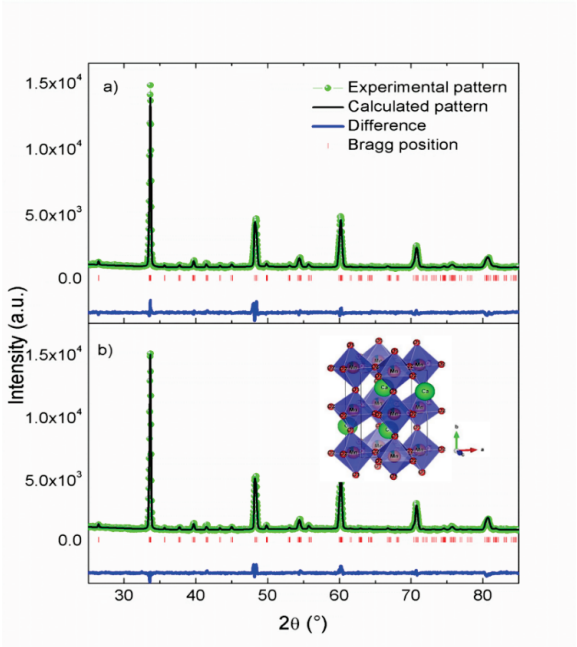

Figure 3. Results of the Rietveld refinement for: a) CMMO-A b) CMMO-B; on inset the scheme of the CMMO structure model.
Source: The Authors.

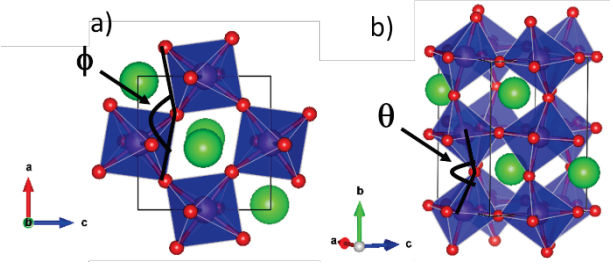

Figure 4. a) ϕ angle to define the rotation angle θ_R and b) θ angle to define the tilt angle θ_T
Source: The Authors.

Table 1.
Lattice parameters obtained by Rietveld Analysis. Ca and O(1) occupy 4c Wyckoff position (x ¼ y), Mn/Mo occupy 4a (0 ½ 0) and O(2) occupy 8d (x y z).

	Sample	CMMO-A	CMMO-B
	a (Å)	5.3503(7)	5.3487(5)
	$b/\sqrt{2}$ (Å)	5.3113(4)	5.3130(2)
	c (Å)	5.3210(9)	5.3206(8)
	V (Å3)	213.84(7)	213.83(6)
Ca	X	0.0383(7)	0.0368(5)
	Z	-0.0084(6)	-0.0010(3)
O(1)	X	0.4871(1)	0.4898(2)
	Z	0.1035(5)	0.0960(7)
O(2)	X	0.2160(5)	0.2075(2)
	Y	-0.0191(4)	-0.0229(5)
	Z	0.2077(8)	0.2087(7)
	d Mn-O(1) X 2	1.958(10)	1.947(7)
	d Mn-O(2) X 2	1.884(8)	1.926(5)
	d Mn-O(2)1 X 2	1.942(8)	1.913(5)
	Mn-Oeq-Mn	160.662(9)	158.400(6)
	σ_{JT}	1.4	3.2
	θ_R	-17.21	-35.68
	θ_T	16.46	15.35
	Rf(%)	7.53	8.91
	χ^2	2.6	2.2

Source: The Authors.

The surface microstructures of CMMO-A and CMMO-B samples are shown in Fig. 5 and Fig. 6. The morphology exhibits a regular and well-defined grain shape in both samples and these are equivalent to that obtained by using conventional synthesis route with resistive furnace [8]. From the figures, it is noted that the grain sizes in CMMO-A and CMMO-B are slightly less than in the previous work [8], such behavior is related to the short time of heat treatment in the present work, whereas the sintering time using resistive furnace is longer and favors grain growth. The micrograph taken at 2000 X for CMMO-A reflect pores and less homogenous surface than in CMMO-B. According to this, the intermediate grinding induces the pore occurrence. The remarkable fact is that the morphology in both cases is similar and corroborate the morphology reported beforehand [8, 16]. The lack of craters in the microstructure of the samples reveals that the energy of the plasma particles that collide with the surface of the samples are not large enough to erode them and allows to preserve the same microstructure exhibited during the synthesis performed in resistive furnace. EDS analysis does not show additional elements (see Table 2). The data reveals that samples have compositions close to the stoichiometric values (Ca 27.24 %, Mn 33.61 %, Mo 6.52 %, O 32.63 %), the slight difference is caused by the bombardment of plasma particles on the surface sample.

Table 2.
Results of EDS analysis.

	CMMO-A		CMMO-B	
	Weight (%)	Sigma	Weight (%)	Sigma
Ca ($K\alpha$)	26.21	1.29	25.35	1.22
Mn ($K\alpha$)	29.33	1.56	28.14	1.46
Mo ($L\alpha$)	9.10	1.29	8.17	1.20
O ($K\alpha$)	35.36	2.38	37.94	2.23

Source: The Authors.

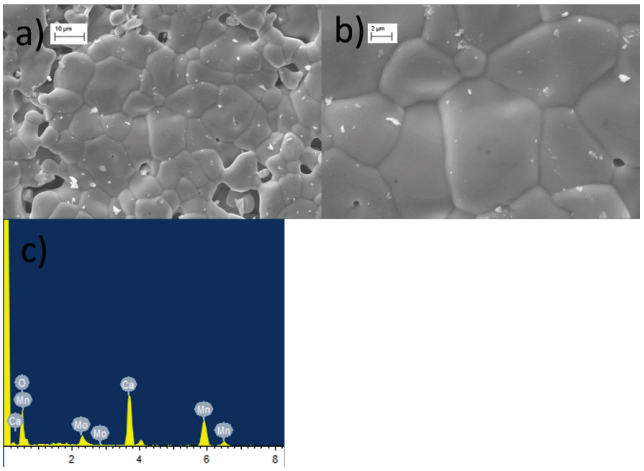

Figure 5. SEM images of CMMO-A sample at a) 2k X b) 5k X with c) EDS analysis.
Source: The Authors.

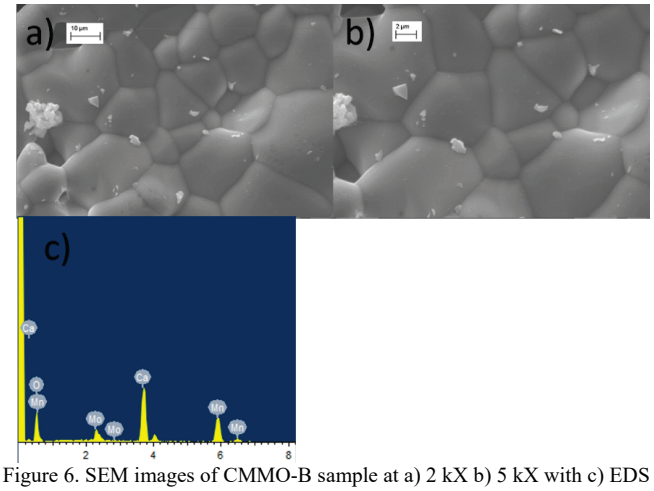

Figure 6. SEM images of CMMO-B sample at a) 2 kX b) 5 kX with c) EDS analysis.
Source: The Authors.

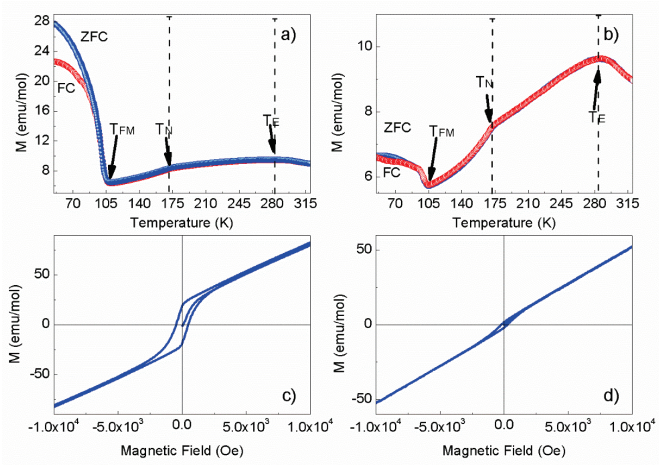

Figure 7. Curve of magnetization as a function of temperature for a) CMMO-A b) CMMO-B. Hysteresis loop recorded at 50 K for c) CMMO-A and d) CMMO-B sample.
Source: The Authors.

Table 3.
Transition temperatures and magnetization values.

Sample	T_N (K)	M (emu/g)	T_E (K)	M (emu/g)	T_{FM} (K)	M at 50 K (emu/g)
CMMO-A	173.9	8.4	279.1	7.5	108.2	27.7
CMMO-B	174.3	9.5	285.5	9.6	101.8	6.6

Source: The Authors.

Magnetic measurements performed on CMMO-A and CMMO-B as a function of temperature in a zero-field-cool (ZFC)- Field cool (FC) cycle under 1kOe and as a function of applied field at 50 K are displayed in Fig. 7. Below ~105 K the ZFC-FC curves exhibits an enhancement of the magnetization for both samples (Fig. 7a and Fig. 7b), the hysteresis loop performed at 50 K shows a weak ferromagnetic (FM) component without magnetic saturation, a larger FM component is evident in the CMMO-A sample than in CMMO-B (Fig. 7c and Fig. 7d). The ZFC-FC curves shows a peak around 174 K and 105 K, these features correspond to the temperature where a structural transition takes place (T) and the Néel temperature (T_N) respectively, according to previous results [10]. The values of magnetization at 50 K, T_N, T_E and the temperature at which the ferromagnetic component arise, T_{FM}, are listed in Table 3.

The values of T_N, T_E with their corresponding magnetization for sample CMMO-B has a value bigger than the sample CMMO-A, with a difference of 0.5 K, 6.4 K and 1.1, 2.1 emu/g respectively. On the other hand, the values of T_{FM} and magnetization at 50 K for sample CMMO-B are lower than the sample CMMO-A, with a difference of 6.6 K and 21.1 emu/g respectively. The difference in these parameters is attributed to differences in the microstructure due to intermediate grinding performed between 700°C and 900°C.

4. Conclusions

CMMO sample was produced by using GD under Argon-Air atmosphere at maximum temperature of 900 °C. According to morphology, the particle shape of samples synthesized by GD is similar in comparison with sample processed by conventional resistive furnace. At room temperature the samples produced by GD exhibit the single-phase indexed with space group Pnma. The lattice parameters, atomic positions, bond lengths, bond angles and tilt angle are similar. The Jahn-Teller distortion and rotation angle are larger when intermediate grinding does not occur. Both samples synthesized by GD exhibit the structural and Neel transition characteristic of this compound. The FM signature is observed in both samples with a reduction of 4 times in its magnitude when intermediate grinding does not take place. In addition, the bombardment of the plasma particles on the samples is not so aggressive as to alter its microstructure at bulk level. The use of GD in this work reduces the time, from 216 to 4 hours and the heat treatment from 1250 to 900 °C in comparison with conventional synthesis route using a resistive furnace.

Acknowledgments

This work was financed by UPTC-DIN under the project No. SGI. 1976. W. Aperador wish to acknowledge the technological support provided by the Universidad Militar Nueva Granada.

References

[1] Mohamed, A., El-Moez, A., Hernando, B. and Ahmed, A.M., Magnetic, magnetocaloric and thermoelectric properties of nickel doped manganites. Journal of Alloys and Compounds, 692, pp. 381-387, 2017. DOI: 10.1016/j.jallcom.2016.09.050

[2] Laouyenne, M.R., Baazaoui, M., Mahjoub, Sa., Cheikhrouhou-Kouba, W. and Oumezzine, M., Enhanced magnetocaloric effect with the high tunability of bismuth in $La_{0.8}Na_{0.2}Mn_{1-x}Bi_xO_3$ ($0 \leq x \leq 0.06$) perovskite manganites. Journal of Alloys and Compounds, 720, pp. 212-220, 2017. DOI: 10.1016/j.jallcom.2017.05.269

[3] Zhou, W., Ma, C., Cao, M., Gan, Z., Wang, X., Ma, Y., Wang, X., Tan, W., Wang, D. and Du, Y., Large magnetocaloric and magnetoresistance effects in metamagnetic $Sm_{0.55}(Sr_{0.5}Ca_{0.5})_{0.45}MnO_3$ manganite. Ceramics International, 43, pp. 7870-7874, 2017. DOI: 10.1016/j.ceramint.2017.03.105

[4] Harsan-Ma, H.J., Zhou, J., Yang, M., Liu, Y., Zeng, S.W., Zhou, W.X., Zhang, L.C., Venkatesan, T., Feng, Y.P. and Ariando, Giant crystalline anisotropic magnetoresistance in nonmagnetic perovskite oxide heterostructures. Physical Review B, 95(15), pp. 155314, 2017. DOI: 10.1103/PhysRevB.95.155314

[5] Li, S.B., Wang, C.B., Liu, H.X., Li, L., Shen, Q., Hu, M.Z. and Zhang, L.M., Effect of sintering temperature on structural, magnetic and electrical transport properties of $La_{0.67}Ca_{0.33}MnO_3$ ceramics prepared by Plasma Activated Sintering. Materials Research Bulletin, 99, pp. 73-78, 2018. DOI: 10.1016/j.materresbull.2017.10.049

[6] Shamblin, J., Heres, M., Zhou, H., Sangoro, J., Lang, M., Neuefeind, J., Alonso, V. and Johnston, S., Experimental evidence for bipolaron condensation as a mechanism for the metal-insulator transition in rare-earth nickelates. Nat. Commun. 9(1), pp. 1-7, 2018. DOI: 10.1038/s41467-017-02561-6

[7] Miclau, M., Grebille, D. and Martin, C., Crystal growth of $CaMn_{1-x}Mo_xO_3$ perovskites by the floating-zone technique ($0 \leqslant x \leqslant 0.15$). Journal of Crystal Growth. 285(4), pp. 661-669, 2005. DOI: 10.1016/j.jcrysgro.2005.08.055

[8] Supelano, G.I., Barón-González, A.J., Buitrago, D.M., Santos, A.S., Parra-Vargas, C.A., Corredor, L.T. and Aguiar, J.A., Structural and magnetic study of $CaMn_{1-x}Mo_xO_3$ (x=0.08, 0.10, 0.12) system. Journal of Superconductivity and Novel Magnetism. 28(1), pp. 259-264 2015. DOI: 10.1007/s10948-014-2855-y

[9] Satadeep, B., Eric, B. and Philippe, G., First-principles study of the dielectric and dynamical properties of orthorhombic $CaMnO_3$. Journal of Physics: Condensed. Matter. 20(25), pp. 255229, 2018. DOI: 10.1088/0953-8984/20/25/255229

[10] Supelano, G.I., Parra-Vargas, C.A., Barón-González, A.J., Santos, A.S. and Frontera, C., Structural study of $CaMn_{1-x}Mo_xO_3$ ($0.08 \leqslant x \leqslant 0.12$) system by neutron powder diffraction. Journal of Alloys and Compounds. 676, pp. 575-581, 2016. DOI: 10.1016/j.jallcom.2016.03.181

[11] Alonso, V., Martínez-Lope, M.J. and Casais, M.T., Evolution of the Jahn-Teller distortion of MnO6 octahedra in $RMnO_3$ perovskites (R=Pr, Nd, Dy, Tb, Ho, Er, Y): a neutron diffraction study. Inorganic Chemistry. 39(5), pp. 917-923, 2000. DOI: 10.1021/ic990921e

[12] Maglia, F., Malavasi, L., Camurlu, H.E., Tacca, A., Chiodelli, G., Spinolo, G., Mozzati, M.C., Anselmi-Tamburini, U. and Munir, Z.A., Synthesis and characterization of pure and doped (Na, Ca, Sr) nanograined $LaMnO_3$ magnetoresistive ceramics. Journal of Nanoscience and Nanotechnology. 8(2), pp. 846-853, 2008. DOI: 10.1166/jnn.2008.B116

[13] Mishra, D.K., Sahu, D.R., Singh, S.K., Mishra, P.K., Pradhan, A.K. and Roul, B.K., Ultrafast sintering of La-Ca-Mn-O bulk ceramics by thermal plasma assisted heating. Journal of Magnetism and Magnetic Materials. 320(8), pp. 1485-1489, 2008. DOI: 10.1016/j.jmmm.2007.12.015

[14] Winchester, M.R. and Payling, R., Radio-frequency glow discharge spectrometry: a critical review. Spectrochimica Acta Part B: Atomic Spectroscopy. 59(5), pp. 607-666, 2004. DOI: 10.1016/j.sab.2004.02.013

[15] Cepeda-Grimaldos, J.F., Santos, A.S. and García, I.S., Low pressure glow discharge I vs. V behavior study, in a DC and pulsed DC in a calorimeter type reactor. Revista Ciencia en Desarrollo 5(1), pp. 7-13, 2014. DOI: 10.19053/01217488.3226

[16] Supelano, G.I., Santos, A.S. and Parra-Vargas, C.A., Effect on structural and magnetic properties of $CaMn_{0.9}Mo_{0.1}O_3$ employing glow discharge in the synthesis route. IEEE. Transaction on Plasma Science. 44(12), pp. 3032-3036, 2016. DOI: 10.1109/TPS.2016.2603783

[17] Szytuła, A., Manganites — Structural aspects, Acta Physica Polonica A. 118(2), pp. 303-306, 2010. DOI: 10.12693/APhysPolA.118.303

I. Supelano-García, received the MSc. degree in Physics in 2015 from Universidad Pedagógica y Tecnológica de Colombia (UPTC-Tunja, Colombia). He is currently a PhD. student of the Physics program at the Universidad Pedagógica y Tecnológica de Colombia (UPTC-Tunja). His research interests are focused on the production and characterization of multiferroic materials.
ORCID: 0000-0002-8020-2686

W.A. Aperador-Chaparro, received the PhD. degree in Materials Engineering from the Universidad del Valle, Colombia. He currently works for Universidad Militar Nueva Granada, Colombia. He is a Volta Group researcher in the Mechatronics Engineering program.
ORCID: 000-0003-1778-0851

C.A. Parra-Vargas, received the PhD. degree from the Universidad Nacional de Colombia, Bogotá. He is currently a professor at the Universidad Pedagógica y Tecnológica de Colombia. His present research interests include low-pressure plasma discharges, materials characterization, and superconductivity.
ORCID: 0000-0001-8968-8654

A. Sarmiento-Santos, received the PhD. degree from the Universidade Federal De Santa Catarina, Florianópolis, Brazil, in 2003. He was a Professor with UIS from 1992 to 1998. He was with the Universidad de Pamplona, Pamplona, Colombia from 2004 to 2006. He presently works for the Universidad Pedagógica y Tecnológica de Colombia. His current research interests include low-pressure plasma discharges, materials characterization, and thin films.
ORCID: 0000-0003-3382-0104